Electronic structure and magnetic properties of higher-order layered nickelates: $La_{n+1}Ni_nO_{2n+2}$ ($n = 4$–6)

Harrison LaBollita and Antia S. Botana
Department of Physics, Arizona State University, Tempe, Arizona 85287, USA

(Received 28 September 2020; revised 20 April 2021; accepted 21 April 2021; published 26 July 2021)

The recent discovery of superconductivity in Sr-doped $NdNiO_2$, with a critical temperature of 10–15 K, suggests the possibility of a new family of nickel-based superconductors. $NdNiO_2$ is the $n = \infty$ member of a larger series of layered nickelates with chemical formula $R_{n+1}Ni_nO_{2n+2}$ (R = La, Nd, Pr; $n = 2, 3, \ldots, \infty$). The $n = 3$ member has been experimentally and theoretically shown to be cupratelike and a promising candidate for superconductivity if electron doping could be achieved. The higher-order $n = 4, 5,$ and 6 members of the series fall directly into the cuprate dome area of filling without the need of doping, thus making them promising materials to study, but have not been synthesized yet. Here, we perform first-principles calculations on hypothetical $n = 4, 5,$ and 6 structures to study their electronic and magnetic properties and compare them with the known $n = \infty$ and $n = 3$ materials. From our calculations, we find that the cupratelike character of layered nickelates increases from the $n = \infty$ to the $n = 3$ members as the charge transfer energy and the self-doping effect due to R-d bands around the Fermi level gradually decrease.

DOI: 10.1103/PhysRevB.104.035148

I. INTRODUCTION

The discovery of high-temperature superconductivity (HTS) in cuprates in 1986 triggered an immense amount of scientific discovery [1]. Yet, despite more than three decades of research, no consensus has emerged for the mechanism of HTS. Among different approaches to address this problem has been to look for materials with similar structures and 3d electron count that are suggested as proxies for cuprate physics. In this regard, focusing on nickelates has been an obvious strategy, as Ni is next to Cu in the periodic table [2,3]. The realization of the promise of nickelates for HTS came with the recent report of superconductivity in Sr-doped $NdNiO_2$ with $T_c \sim 10$–15 K [4,5]. This observation not only constitutes the realization of the first superconducting nickel-oxide material, but also bolsters studying other layered nickelates—$NdNiO_2$ is simply one of the members of a larger family of materials [6,7].

This low-valence layered nickelate family is represented by the general formula $R_{n+1}Ni_nO_{2n+2}$ (R = La, Nd, Pr; $n = 2, 3, \ldots, \infty$) in which each member contains n-NiO_2 layers, in analogy to the CuO_2 planes of cuprates (see Fig. 1). Layered nickelates are obtained via oxygen reduction from the corresponding parent perovskite or Ruddlesden-Popper (RP) phases [6–8]. As of now, only the $n = 2$, 3, and ∞ layered nickelates have been experimentally realized. $NdNiO_2$ (112) is the $n = \infty$ member of the series and realizes the hard-to-stabilize Ni^{1+}: d^9 oxidation state [4,9–12]. Superconductivity in this material is reached upon hole doping with Sr that drives the electron count into the cuprate dome area of filling (with maximum T_c obtained at $d^{8.8}$ filling) [5]. This discovery has attracted a great deal of experimental [13–20] and theoretical [21–39] attention. The $n = 2$ member ($R_3Ni_2O_6$: 326) is far from cuprates in terms of electron count [6,40,41], so we will not study it here. The $n = 3$ phases ($R_4Ni_3O_8$: 438), with an average Ni valence of 1.33+ ($d^{8.67}$), fall into the overdoped regime of cuprates in terms of electron count and, as such, are not superconducting even though they have been shown to be one of the closest cuprate analogs to date [42,43]. Both of these nickelates (R438s and R112s) have their own respective shortcomings. In order to reach the dome area of d filling, the 112 materials must be hole doped, which is known to cause structural disorder in the samples [4,14], and the 438 materials must be electron doped, which is yet to be successfully done.

In contrast, the $n = 4$, 5, and 6 members of the series would all fall into the cuprate dome in terms of electron count without the need of doping and are hence very promising materials to pursue. Starting with the $n = 4$ compound ($R_5Ni_4O_{10}$: 5410), it would have an average Ni valence of 1.25+ ($d^{8.75}$). The $n = 5$ material ($R_6Ni_5O_{12}$: 6512) would have an average Ni valence of 1.2+ ($d^{8.80}$). Lastly, the $n = 6$ compound ($R_7Ni_6O_{14}$: 7614) would have an average Ni valence of 1.17+ ($d^{8.83}$) (see Fig. 1). Even though $n = 4$–6 reduced nickelates have yet to be experimentally realized, prospects seem bright as growth of parent La-based RP $n = 4$–5 phases has been recently reported [44,45]. All of these parent higher-order RP samples correspond to thin films grown via molecular beam epitaxy (MBE)—obtaining bulk samples will likely be difficult due to thermodynamic instabilities.

Here, we use first-principles calculations to describe the electronic structure of hypothetical $n = 4$–6 layered nickelates ($R_5Ni_4O_{10}$, $R_6Ni_5O_{12}$, and $R_7Ni_6O_{14}$ with R = La), exploiting the prospect that their parent RP phases can be reduced. We then compare the electronic structure of these layered $n = 4$–6 materials to the known $n = 3$ and $n = \infty$ members of the series. We find that a low-spin state for Ni is

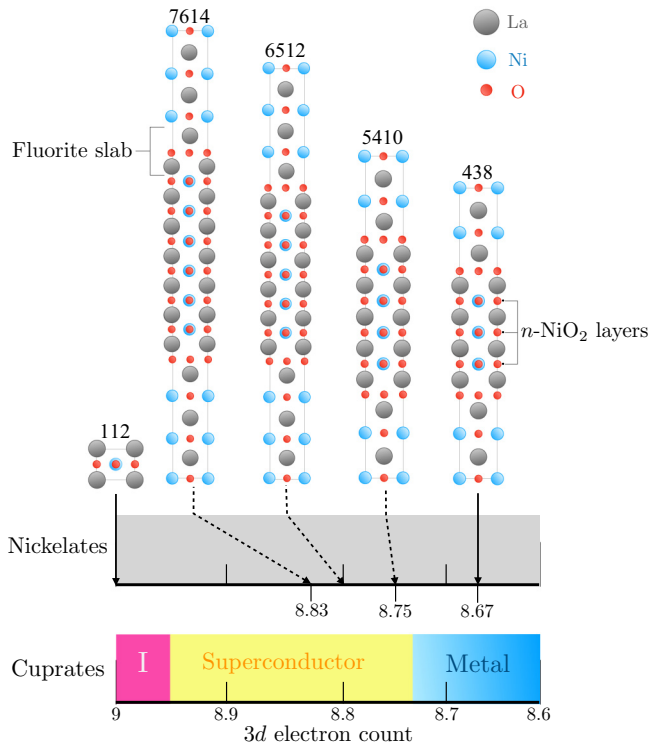

FIG. 1. Schematic phase diagram of layered nickelates (top) and cuprates (bottom) presented as a function of 3d electron count (I, insulator). For nickelates, only a couple line compositions are known in the range of 3d electron count shown: $RNiO_2$ (112; $n = \infty$) and $R_4Ni_3O_8$ (438; $n = 3$). Dashed lines stand for $R_5Ni_4O_{10}$ (5410; $n = 4$), $R_6Ni_5O_{12}$ (6512; $n = 5$), and $R_7Ni_6O_{14}$ (7614; $n = 6$), which have not been synthesized yet. The structure of each of these materials is also shown. All systems contain n-NiO_2 layers, and the $n = 3$–6 systems also exhibit a blocking fluorite slab.

the preferred ground state for $n = 4$–6 compounds, in analogy to the 438 materials and cuprates. The R-d bands (which have been reported to be relevant for the low-energy physics of the 112 materials) start playing a role in the electronic structure of layered nickelates when gradually moving from the $n = 3$ to the $n = 6$ members. Importantly, the charge transfer energy of these compounds gradually decreases when going from $n = \infty$ to $n = 3$. All in all, the cupratelike character of low-valence layered nickelates is found to decrease with n.

II. COMPUTATIONAL METHODS

Electronic structure calculations were performed using the all-electron, full potential code WIEN2K [46] based on the augmented plane wave plus local orbitals (APW + lo) basis set. The Perdew-Burke-Ernzerhof version of the generalized gradient approximation (GGA) [47] was used for the nonmagnetic calculations. Additionally, we perform GGA + U [48] calculations to account for the missing correlations for the Ni-d states. We employ two double counting schemes in the GGA + U calculations: "fully localized limit" (FLL) and "around mean field" (AMF). For both schemes we studied the evolution of the electronic structure with increasing U ($U = 1.5$–5.5 eV). We have chosen a nonzero $J = 0.7$ eV in our calculations to properly account for the anisotropy of the interaction [49].

TABLE I. Calculated lattice parameters for higher-order La-based nickelates (5410, 6512, and 7614), as well as experimental 438 [7] and 112 [10] lattice parameters. All values are given in angstroms.

n	Material	a	b	c
3	La438	3.97	3.97	26.1
4	La5410	3.97	3.97	32.9
5	La6512	3.96	3.96	39.9
6	La7614	3.97	3.97	46.1
∞	La112	3.95	3.95	3.37

We have chosen to study all layered nickelates with R = La to avoid ambiguities in the treatment of the 4f states that would arise from Nd or Pr. We note that in 112 nickelates, the La variant is, as of now, not superconducting upon hole doping (in contrast to the Pr and Nd counterparts) [4] even though the electronic structure of $LaNiO_2$ and $NdNiO_2$ is essentially the same except for the f bands [32]. The same conclusion about the similarity of the electronic structure upon R substitution applies to the higher-order $n = 4$–6 materials. For La438, La5410, and La6512, we used a k mesh of $10 \times 10 \times 10$ k points in the irreducible Brillouin zone, while for La7614 a k mesh of $12 \times 12 \times 12$ k points and for La112 a k mesh of $9 \times 9 \times 11$ $k$points was required for convergence. We used $R_{MT}K_{max} = 7.0$ and muffin-tin radii 2.50, 1.99, and 1.72 Å for La, Ni, and O, respectively, for all of our calculations.

III. STRUCTURAL PROPERTIES

We construct the structure of hypothetical La-based $n = 4$–6 nickelates using the structure of the $La_4Ni_3O_8$ material as a reference. The structure of 438 materials is tetragonal (with an $I4/mmm$ space group) and contains three NiO_2 planes separated by a single layer of R ions, similar to the 112 materials. However, in contrast to infinite-layer nickelates (with $P4/mmm$ space group), in the 438 materials, the NiO_2 planes are separated along the c axis by a fluoritelike RO blocking slab (see Fig. 1) that makes the intertrilayer coupling very weak (this fluorite slab is absent in the 112 phase). We safely assume that higher-order nickelates will have an analog structure to that of the 438 materials once synthesized, i.e., tetragonal with an $I4/mmm$ space group, n-NiO_2 planes along c, and fluorite slabs formed by the rare-earth and oxygen ions as spacing layers. With these considerations, we have all of the ingredients to construct the structure for each of the reduced La-based $n = 4$–6 higher-order phases. We then optimize the lattice parameters and internal coordinates for each phase. Our optimizations were done using a ferromagnetic configuration within GGA, the ground state for these systems (see below).

The optimized lattice parameters for each higher-order phase are shown in Table I, and the experimental ones for La438 and La112 compounds are also shown as a reference. The in-plane lattice parameters are almost identical for all compounds, whereas the out-of-plane lattice parameter obviously increases with the number of layers. Relevant bond lengths are consistent for all compounds: $d_{Ni\text{-}O} = 1.97$–

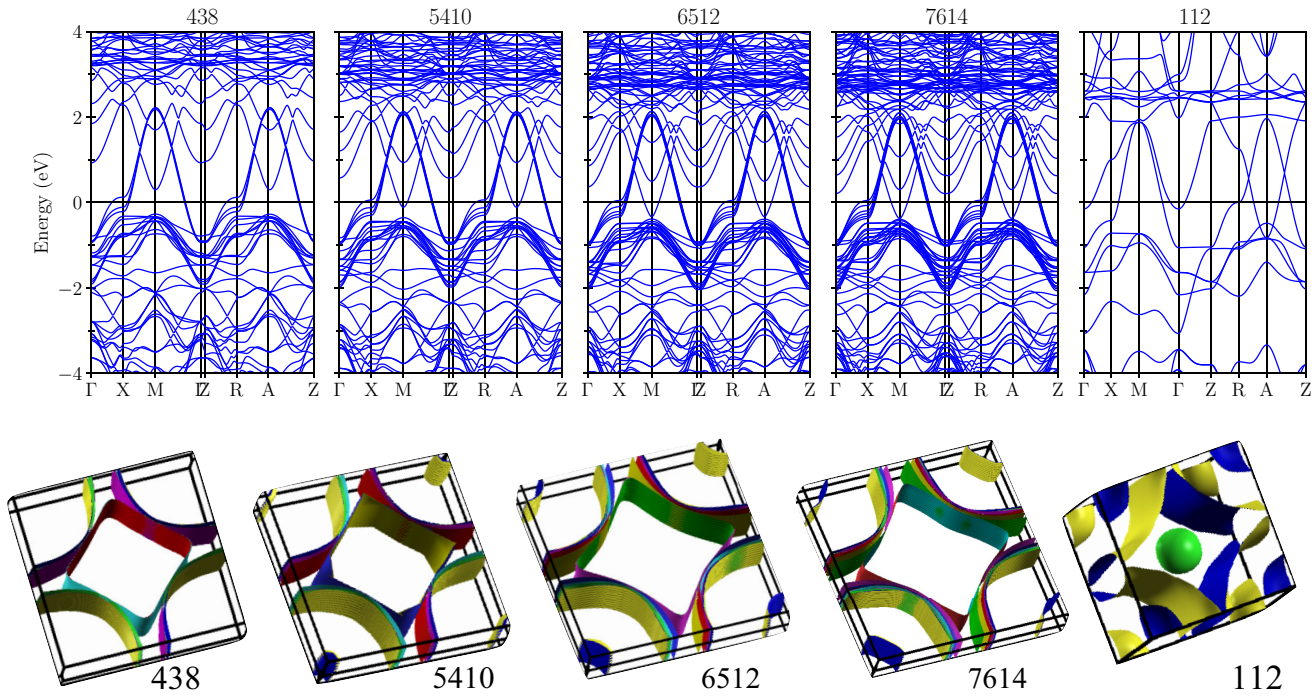

FIG. 2. Top panels: nonmagnetic band structures for the La-based 438 ($n = 3$), 5410 ($n = 4$), 6512 ($n = 5$), and 7614 ($n = 6$) layered nickelates (with $I4/mmm$ space group) and for the 112 ($n = \infty$) compound (with $P4/mmm$ space group) within GGA. Bottom panels: Corresponding Fermi surface for each compound.

1.99 Å, $d_{\text{La-Ni}} = 3.15$–3.26 Å, and $d_{\text{La-O}} = 2.51$–2.59 Å. From our structural relaxations, we find the obtained bond lengths agree well with the experimentally derived values for the La438 and La112 compounds, which serves as a benchmark for our relaxations in the $n = 4$–6 structures [7,50].

IV. NONMAGNETIC CALCULATIONS

Figure 2 shows the nonmagnetic band structures and corresponding Fermi surfaces of the La-based $n = 4$–6 nickelates after the structural relaxations. The band structures and Fermi surfaces for La438 and La112 using the experimental structural data are shown as a reference. In cuprates, a single band of $d_{x^2-y^2}$ character hybridized with O-p states is active in the vicinity of the Fermi level. For the La112 compound (at d^9 filling), in addition to the $d_{x^2-y^2}$ band, there are also La-5d bands crossing the Fermi level at both A (with dominant d_{xy} character) and Γ (with d_{z^2} character). As such, the corresponding Fermi surface of the 112 material contains not only a cylinder with Ni-$d_{x^2-y^2}$ holes, but also an electronlike spherical pocket in the center (Γ, with La-d_{z^2} character) and another electronlike sphere at each corner (A, with La-d_{xy} character). This has been described in earlier literature, and quite some attention has been paid to the role of R-d bands, as they make the electronic structure and fermiology noncupratelike in R112 materials [3,21,22,38,51].

The evolution of the electronic structure of La-based layered nickelates from $n = \infty$ to $n = 3$ shows one $d_{x^2-y^2}$ band per Ni crossing the Fermi level for each material, as expected (see Fig. 2), with a bandwidth that does not significantly change with n. In the multilayered systems ($n = 3$–6), a splitting between the Ni-$d_{x^2-y^2}$ bands is observed at X as a consequence of interlayer hopping, similar to that in multilayer cuprates [52]. The most important difference as n increases is the gradual involvement of La-d bands. In the 438 ($n = 3$) compound the situation is very similar to that in the cuprates: There is a single $d_{x^2-y^2}$ band per Ni crossing the Fermi level, with no La-d involvement, as reported before [42]. In La5410, La-d bands start crossing the Fermi level giving rise to electron pockets at A and M, and they gradually shift down to lower energies for La6512 and La7614. Unlike in the 112 material, there is no La-d band crossing at Γ.

These differences in electronic structure can be easily appreciated in the corresponding Fermi surfaces also shown in Fig. 2. In La438 ($n = 3$) the Fermi surface consists of three Ni-$d_{x^2-y^2}$-derived pockets only: the bonding, nonbonding, and antibonding superpositions of the three layers. The outer hole-like pockets centered around the zone corner correspond to the lower-lying bands, while the inner pocket (nearly square-like around Γ) arises from the antibonding (higher-lying) band. These Ni-$d_{x^2-y^2}$-derived pockets are kept in the $n = 4$–6 materials—with extra hole pockets centered around the zone corner as the number of Ni-$d_{x^2-y^2}$ bands crossing the Fermi level increases with n. The important difference arises from the La-d bands crossing the Fermi level at A and M in the $n = 4$–6 systems mentioned above—the La-d electronlike spherical pocket at A in the 112 compound becomes cylindrical in the $n = 4$–6 materials. The size of this cylindrical pocket increases with n. The small spherical pocket at Γ in the 112 compound is absent in the $n = 4$–6 materials (as mentioned above, unlike in the 112 material, there is no La-d band crossing at Γ in the $n = 4$–6 systems). One should note that the structure of the $n = 3$–6 nickelates is different from that of the infinite-layer material as the former have a fluorite blocking

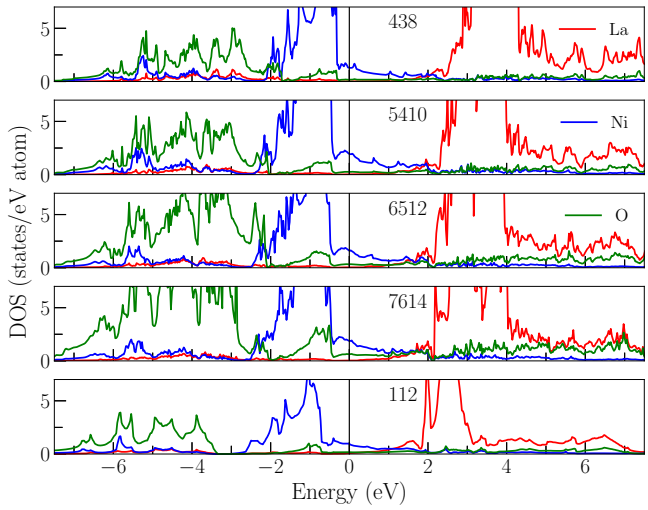

FIG. 3. Comparison of the total nonmagnetic atom-resolved density of states for the La, Ni, and O ions in La-based 438 ($n = 3$), 5410 ($n = 4$), 6512 ($n = 5$), 7614 ($n = 6$), and 112 ($n = \infty$) layered nickelates within GGA.

layer that cuts the c-axis dispersion and causes the changes in the electronic structure and fermiology we have described. Importantly, the Fermi surfaces of the $n = 3$–6 nickelates are very similar to those of multilayered cuprates (see, for example, Ref. [52]), except for the additional contributions from the R-d bands in the $n = 4$–6 compounds.

To gain a complete description of the nonmagnetic electronic structure, Fig. 3 shows the atom-resolved densities of states (DOSs) for the La, Ni, and O ions within GGA for $n = \infty$ and $n = 3$–6 layered nickelates. The density-of-states plots confirm the above description and clearly show how the La-5d states shift down in energy as n increases. The centroid of the Ni-d states does not significantly change across the series. In contrast, the O-p centroid shifts to lower energies (away from the Fermi level) when going from the La438 compound to the La112 compound, by ∼1 eV across the series. As a consequence, the degree of p-d hybridization increases gradually from La112 to La438 [53]. In connection to this, studies of 112 materials have highlighted their much larger charge transfer energy ($\Delta = \varepsilon_d - \varepsilon_p$) with respect to cuprates ($\Delta_{112} \sim 4$ eV, whereas prototypical cuprate values are ∼2 eV [54]). This is a relevant parameter in cuprates, as many theories of HTS in cuprates are based on the large degree of p-d hybridization, which ultimately allows for Zhang-Rice singlet formation [55]. Importantly, a decreasing charge transfer energy across cuprates has been shown to result in higher T_c values [54]. To obtain a quantitative estimate for each nickelate, explicit Δ values are obtained following Ref. [56] using band centroids (for Ni $d_{x^2-y^2}$ and O $p\sigma$) calculated as

$$E_i = \frac{\int E g_i(E)\, dE}{\int g_i(E)\, dE}, \tag{1}$$

where $g_i(E)$ is the partial density of states for orbital i. An ambiguity can inevitably be introduced in determining the integration range—we set it to cover the bonding-antibonding band complex for Ni-$d_{x^2-y^2}$ states, and the DOS range for O-$p\sigma$ states. The values obtained for the centroids in 112 and 438 materials using such integration limits are similar to the on-site energies of the corresponding maximally localized Wannier functions reported in the literature [38,57].

TABLE II. Estimates of the on-site energies of the Ni-$d_{x^2-y^2}$ and O-p_σ orbitals from the DOSs and the estimated charge transfer energy. Additionally, we include estimates of the charge transfer energy obtained via Wannierizations for the $n = 3$, 4, and ∞ compounds using WANNIER90 [59] and WIEN2WANNIER [60].

n	$E_{\text{O-}p\sigma}$ (eV)	$E_{\text{Ni-}d_{x^2-y^2}}$ (eV)	Δ_{DOS} (eV)	Δ_{Wannier} (eV)
3	−4.53	−1.02	3.52	3.52 (Ref. [57])
4	−4.65	−1.04	3.61	3.80 (Ref. [58])
5	−4.79	−1.07	3.72	
6	−4.85	−1.05	3.80	
∞	−5.51	−1.12	4.39	4.40 (Ref. [38])

The derived average centroid energies with respect to the Fermi level for Ni-$d_{x^2-y^2}$ and O-p_σ orbitals, as well as estimated charge transfer energies, are summarized in Table II. The average charge transfer energy for each material increases with n with an overall increase of ∼1 eV as could be inferred from the DOSs. As mentioned above, many theories of HTS in cuprates are based on their small charge transfer energy. If this is a relevant parameter in layered nickelates as well, $n = 3$–6 phases should then be promising materials to explore.

Figure 4 shows the charge transfer energy (average and layer dependent) versus doping $x = 1/n$. This plot reflects that a linear fit to the average charge transfer energy is good, even though it shows some slight deviations, indicating some sensitivities in our estimates. The 112 nickelate has effectively a single layer, the 438 and 5410 compounds have inner and outer layers, and the 6512 and 7614 have inner, next-to-inner, and outer layers. Interestingly, we find that the charge transfer energy is layer dependent in a systematic manner within each material: larger on the inner NiO_2 layers, decreasing gradually when moving outwards.

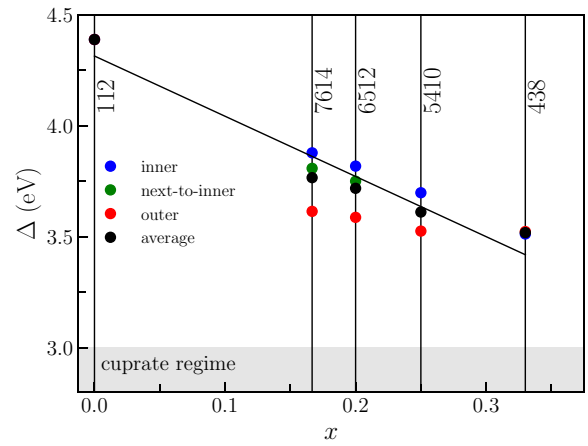

FIG. 4. Charge transfer energies (average and layer dependent) plotted vs doping level ($x = 1/n$) for each La-based layered nickelate ($x = 0$ for La112, $x = 0.17$ for La7614, $x = 0.2$ for La6512, $x = 0.25$ for La5410, and $x = 0.33$ for La438).

V. MAGNETIC CALCULATIONS

Using spin-polarized calculations, we have performed a full study of the stability of different spin states for different magnetic configurations in all layered nickelates constructing $\sqrt{2} \times \sqrt{2}$ supercells (with *Cmmm* space group).

Concerning possible Ni spin states in these materials, one should start by considering that, for $n = 3$–6 nickelates, the Ni ions sit in a square-planar environment with an average d filling that can be described as $d^{8+\delta}$ (with δ increasing with n). This is also effectively the picture in the $n = \infty$ compound (even though a simple ionic count gives a Ni^{1+}: d^9) due to the self-doping effect from R-d bands. Importantly, there are two possible spin states for such a Ni: low spin (LS) and high spin (HS). These two possibilities arise from the competition between the crystal field splitting Δ_{CF} in the e_g states and Hund's rule coupling J_H. The LS state (with Δ_{CF} larger than J_H) corresponds to a d filling $(t_{2g})^6(d_{z^2})^2(d_{x^2-y^2})^\delta$ with $S = \delta/2$ and moment of δ per nickel. The HS configuration (with J_H larger than Δ_{CF}) corresponds to a d filling $(t_{2g})^6(d_{z^2,\uparrow})^1(d_{x^2-y^2,\uparrow})^1\ (d_{z^2,\downarrow})^\delta$ with $S = (2-\delta)/2$ and a moment of $2-\delta$ per nickel. Understanding the preferred spin state is crucial to understanding the physics of these materials. Specifically, a HS spin state is noncupratelike as it involves Ni-d_{z^2} states around the Fermi level, while a LS spin state is cupratelike with the involvement of Ni-$d_{x^2-y^2}$ states only.

In order to find the ground state for each compound, we first compare the energies of the antiferromagnetic (AFM), ferromagnetic (FM), and nonmagnetic states at the GGA level. Within GGA, the energy of the nonmagnetic state for all compounds is higher compared with both the AFM and FM configurations by 10–60 meV/Ni. The energy differences and Ni magnetic moments (LS for all materials) from GGA calculations on $n = 3$–6 and ∞ nickelates are shown in Appendix A, Table III.

Given that the nonmagnetic state is higher in energy than the FM or AFM in all materials, we investigate the relative stability between the latter states at the GGA + U level with the two double counting schemes mentioned above (AMF and FLL). We note that AMF and FLL are known to stabilize different spin states: FLL tends to stabilize HS states, whereas AMF tends to penalize magnetic energies and hence has a tendency to stabilize LS states instead [49]. The energy differences ($E_{AFM} - E_{FM}$) and Ni magnetic moments for each compound from all of our GGA + U calculations have been tabulated in Appendix A, Tables IV (FLL) and V (AMF). In a high-spin configuration for the Ni-$d^{8+\delta}$ ions (with half-filled $d_{x^2-y^2}$ bands) an AFM checkerboard configuration is preferred. In contrast, the low-spin Ni-$d^{8+\delta}$ ions (with $d_{x^2-y^2}$ bands away from half filling) prefer a FM order. Within both the AMF and FLL schemes, our calculations show that a LS-FM ground state is preferred for the $n = 4$–6 compounds. The stability of this state has been confirmed using fixed spin moment calculations. This makes these higher-order phases similar to the R438 ($n = 3$) material, for which a LS-FM ground state is also obtained from first-principles calculations that has been shown to be consistent with polarized x-ray absorption experiments [42]. The LS state is metallic, with all Ni moments remaining below 1 μ_B and the involvement of Ni bands of $d_{x^2-y^2}$ character only around the Fermi level

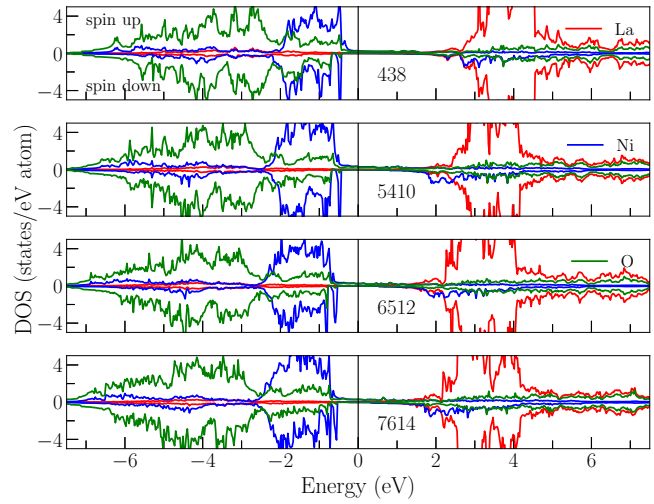

FIG. 5. Comparison of the atom-resolved densities of states for the La, Ni, and O ions in La-based 438 ($n = 3$), 5410 ($n = 4$), 6512 ($n = 5$), and 7614 ($n = 6$) layered nickelates in their LS-FM metallic ground state within GGA + U (AMF) for $U = 5.5$ eV.

(see below). In contrast to $n = 3$–6 materials, for La112 ($n = \infty$) we find instead an AFM ground state with a LS-to-HS transition upon increasing U, in agreement with previous literature [3,38,61]. This AFM state in La112 remains metallic up to the highest U value used and is fundamentally different due to the involvement of a flat Ni-d_{z^2} band (in addition to the $d_{x^2-y^2}$) at the Fermi level [62].

For metallic R438, the AMF scheme has been shown to give a description of the electronic structure that is in much better agreement with experiments [42]. Given their similarities, we expect the same for the $n = 4$–6 materials, so we adopt this scheme to describe the electronic structure of their LS metallic ground state. Figure 5 shows the atom-resolved densities of states for the La, Ni, and O ions for $n = 4$–6 nickelates in their ground state (for a standard U for Ni of 5.5 eV [42,63,64]); for the corresponding band structures, see Fig. 6 in Appendix B. The most important feature of the solution we have obtained for $n = 4$–6 materials is the LS state nature of the Ni ions with the sole involvement of one Ni-$d_{x^2-y^2}$ band per Ni around the Fermi level. As mentioned above, this contrasts with the nature of the high-spin AFM ground state obtained in the $n = \infty$ compounds [61,62], which is characterized by a multiorbital nature with Ni-d_{z^2} states pinned at the Fermi level playing a crucial role. In all cases ($n = 4$–6 and ∞), R-d bands still cross the Fermi level, but the LS ground state of the $n = 4$–6 materials is more cupratelike in nature as only Ni-$d_{x^2-y^2}$ states play a role in the low-energy physics. Overall, the trends with n of the electronic structure in the LS state are similar to those of the nonmagnetic state: (i) There is a shift of the La-5d states to lower energies as n increases across the series (more evident in Fig. 6), (ii) the centroid of the Ni-d states remains nearly fixed throughout the series, and (iii) the O-p states shift to lower energies with increasing n (by ∼1 eV across the series). As discussed earlier, these effects collectively decrease the degree of p-d hybridization as n increases.

Concerning the LS-FM nature of the ground state we have described for $n = 4$–6 materials, it is important to note that antiferromagnetic states are observed in cuprates near d^9 filling (indeed, we find an AFM ground state for the $n = \infty$ material). However, when hole doped away from d^9, one finds broken-symmetry phases in both the cuprates and layered nickelates [65–68]. While we have obtained a LS-FM ground state for $n = 4$–6 nickelates, earlier work on R438s ($n = 3$) found that this LS state does in fact compete in energy with a charge and spin stripe phase [42,69]. With the higher-order $n = 4$–6 materials exhibiting a similar electronic structure to the R438s ($n = 3$), we anticipate that such broken-symmetry phases or even complex magnetic behavior [70] may be present in these materials as well. Given that charge and spin stripe phases would require large supercells, their analysis is beyond the scope of this work, and we leave this for future calculations and experimental observations. We point out that a nesting-driven density wave transition has actually been previously commented on by Poltavets *et al.* [71] for the $n = 3$ nickelate based on its fermiology. Given that the Fermi surfaces of the $n = 3$ and $n = 4$–6 materials are indeed similar (see Fig. 2), this can be a likely possibility in these latter phases as well.

Finally, even though the AFM state is not the ground state in $n = 4$–6 materials, we briefly describe some interesting aspects of it here. First, a LS-to-HS transition with U is obtained within both AMF and FLL schemes (akin to that in La112). However, in contrast to La112, at high enough U values this AFM state in $n = 3$–6 nickelates is insulating, specifically, at $U \sim 2.7$ eV for La438 and $U \sim 5.5$ eV for La5410, La6512, and La7614. We attribute the possibility to open up a gap in the AFM state in $n = 3$–6 materials (in stark contrast to the 112s) to the existence of the blocking fluorite slab that cuts the d_{z^2} off-plane hopping. Interestingly, in the AFM state for $n = 4$–6 nickelates there is a tendency for the moments to disproportionate between inner and outer layers, with disproportionation being more pronounced in the La5410 and La7614 cases, which lack a mirror plane. The higher Ni moments are found at the inner layers and gradually decrease moving outwards. This effect is present in both double counting schemes; the FLL scheme only exacerbates it (see Appendix A, Table IV). This disproportionation effect has been seen before in multilayered cuprates, where there is a charge imbalance between the inner and outer planes [72–76].

VI. CONCLUSIONS

We have used first-principles calculations to study the electronic and magnetic properties of hypothetical La-based $n = 4$–6 layered nickelates and compared them with those of the known $n = 3$ and $n = \infty$ materials. Our calculations show a gradual increase in cupratelike behavior as n increases in these low-valence layered nickelates. In particular, we find that a low-spin state for Ni is the preferred ground state of the $n = 4$–6 compounds analogous to the 438 materials and cuprates. The self-doping effect due to R-d bands and the charge transfer energy of these materials gradually increase with n. As many theories of HTS in cuprates are based on their large degree of p-d hybridization (small charge transfer energy), we argue that $n = 3$–6 layered nickelates are then very promising materials to study in this context.

ACKNOWLEDGMENT

We thank M. R. Norman for fruitful discussions. We acknowledge the support from Grant No. NSF-DMR 2045826 and from the ASU Research Computing Center for high-performance computing (HPC) resources.

APPENDIX A: ENERGIES AND MAGNETIC MOMENTS

The energy differences between different magnetic configurations within GGA and GGA + U calculations are described in this Appendix. Table III shows the results from our GGA calculations. We include the Ni magnetic moments for both AFM and FM spin configurations, as well as energy differences between the nonmagnetic (NM) and AFM or FM states. In all cases, the FM and/or AFM states are favored over the NM state across the series. The results from our GGA + U calculations are summarized in Tables IV and V. In Table IV, we provide the energy differences between the AFM state and the FM state with GGA + U for a range of U values with the FLL double counting scheme. A qualitative description of

TABLE III. Energy differences (in meV/Ni) between nonmagnetic and antiferromagnetic (AFM) or ferromagnetic (FM) spin configurations within GGA for $n = 3$–6 and ∞ materials. Additionally, the magnetic moments (MMs) for both the antiferromagnetic and ferromagnetic spin configurations are shown for Ni atoms in each distinct layer. Magnetic moments are in μ_B.

Material	$E_{NM} - E_{AFM}$ (meV/Ni)	$E_{NM} - E_{FM}$ (meV/Ni)	NiO_2 layer	AFM MM	FM MM
La438	6.36	23.32	inner	0.30/−0.30	0.51
			outer	0.27/−0.27	0.50
La5410	25.52	19.52	inner	0.44/−0.44	0.51
			outer	0.34/−0.33	0.49
La6512	40.51	13.92	inner	0.54/−0.54	0.44
			next-to-inner	0.48/−0.48	0.47
			outer	0.37/−0.37	0.49
La7614	66.25	16.79	inner	0.59/−0.59	0.46
			next-to-inner	0.51/−0.51	0.52
			outer	0.39/−0.39	0.55
La112	66.81	−2.04		0.68/−0.68	0.31

TABLE IV. GGA + U (FLL). Energy differences (in meV/Ni) between a checkerboard antiferromagnetic (AFM) and ferromagnetic (FM) state for La-based layered nickelates with $n = 3, 4, 5, 6$, and ∞ within GGA + U as a function of U using the FLL double counting scheme. A positive energy difference indicates the FM state is energetically favored, while a negative difference indicates the AFM state is favored. A qualitative description of the ground state (GS) of the system at each value of U is provided. Finally, the Ni magnetic moments for both AFM and FM spin configurations are given for each Ni in each layer. Blank entries in the last column indicate a calculation that could not be converged.

U (eV)	$E_{\mathrm{AFM}} - E_{\mathrm{FM}}$ (meV/Ni)	GS	NiO_2 layer	AFM moments (μ_B)	FM moments (μ_B)
			La438		
1.5	−13.8	HS-AFM metal	inner	1.1/−1.1	0.68
			outer	0.92/−0.92	0.67
2.7	−107.6	HS-AFM insulator	inner	1.3/−1.3	0.72
			outer	1.1/−1.1	0.71
4.0	−216.9	HS-AFM insulator	inner	1.4/−1.4	1.3
			outer	1.2/−1.2	0.87
5.5	−281.7	HS-AFM insulator	inner	1.4/−1.4	1.5
			outer	1.3/−1.3	1.3
			La5410		
1.5	91.5	LS-FM metal	inner	0.97/−0.97	0.76
			outer	0.54/−0.56	0.73
2.7	114.8	LS-FM metal	inner	1.2/−1.2	0.80
			outer	0.71/−0.71	0.77
4.0	59.9	LS-FM metal	inner	1.3/−1.3	0.84
			outer	0.78/−0.78	0.81
5.5	79.2	HS-FM metal	inner	1.4/−1.4	1.4
			outer	0.93/−0.93	1.3
			La6512		
1.5	48.1	LS-FM metal	inner	0.69/−0.69	0.80
			next-to-inner	0.65/−0.65	0.78
			outer	0.55/−0.54	0.75
2.7	134.7	LS-FM metal	inner	0.90/−0.90	0.85
			next-to-inner	0.82/−0.82	0.83
			outer	0.69/−0.70	0.79
4.0	79.6	LS-FM metal	inner	1.2/−1.2	0.89
			next-to-inner	0.61/−0.61	0.88
			outer	1.2/−1.2	0.84
5.5	19.5	LS-FM metal	inner	1.3/−1.3	0.94
			next-to-inner	0.57/−0.57	0.92
			outer	1.3/−1.3	0.87
			La7614		
1.5	13.4	LS-FM metal	inner	0.89/−0.89	0.83
			next-to-inner	0.64/−0.64	0.80
			outer	0.63/−0.63	0.76
2.7	56.3	LS-FM metal	inner	1.1/−1.1	0.87
			next-to-inner	0.64/−0.64	0.85
			outer	1.1/−1.1	0.81
4.0	32.8	LS-FM metal	inner	1.2/−1.2	0.92
			next-to-inner	0.67/−0.67	0.90
			outer	1.2/−1.2	0.85
5.5			inner	1.3/−1.3	
			next-to-inner	0.66/−0.66	
			outer	1.3/−1.3	
			La112		
1.5	−143.8	LS-AFM metal		0.83/−0.83	0.87
2.7	−138.5	HS-AFM metal		1.04/−1.04	0.93
4.0	−146.4	HS-AFM metal		1.1/−1.1	0.99
5.5	−135.4	HS-AFM metal		1.2/−1.2	1.1

TABLE V. GGA + U (AMF). Energy differences (in meV/Ni) between a checkerboard antiferromagnetic and ferromagnetic state for La-based layered nickelates with $n = 3$, 4, 5, 6, and ∞ within GGA + U as a function of U using the AMF double counting scheme. A positive energy difference indicates the FM state is energetically favored, while a negative difference indicates the AFM state is favored. A qualitative description of the ground state (GS) of the system at each value of U is provided. Finally, the Ni magnetic moments for both AFM and FM spin configurations are given for each Ni in each layer. In the 112 material, in spite of the moments remaining below 1 μ_B within AMF at all U's, already for a low U value, a d_z^2 band is pinned at the Fermi level, as in the HS state described in Refs. [61,62] obtained within FLL.

U (eV)	$E_{\mathrm{AFM}} - E_{\mathrm{FM}}$ (meV/Ni)	GS	NiO_2 layer	AFM moments (μ_B)	FM moments (μ_B)
			La438		
1.5	17.4	LS-FM metal	inner	0.86/−0.86	0.67
			outer	0.70/−0.69	0.66
2.7	38.6	LS-FM metal	inner	1.2/−1.2	0.68
			outer	1.1/−1.1	0.67
4.0	16.0	LS-FM metal	inner	1.3/−1.3	0.68
			outer	1.1/−1.1	0.67
5.5	49.4	LS-FM metal	inner	1.4/−1.4	0.67
			outer	1.2/−1.2	0.66
			La5410		
1.5	13.5	LS-FM metal	inner	0.72/−0.72	0.74
			outer	0.49/−0.50	0.71
2.7	80.9	LS-FM metal	inner	1.1/−1.1	0.75
			outer	0.57/−0.57	0.72
4.0	42.6	LS-FM metal	inner	1.2/−1.2	0.74
			outer	0.47/−0.45	0.71
5.5	25.3	LS-FM metal	inner	1.3/−1.3	0.73
			outer	0.38/−0.38	0.69
			La6512		
1.5	43.5	LS-FM metal	inner	0.66/−0.66	0.78
			next-to-inner	0.62/−0.62	0.76
			outer	0.52/−0.52	0.73
2.7	133.3	LS-FM metal	inner	0.73/−0.73	0.78
			next-to-inner	0.68/−0.68	0.77
			outer	0.59/−0.59	0.73
4.0	195.4	LS-FM metal	inner	0.75/−0.75	0.78
			next-to-inner	0.72/−0.72	0.76
			outer	0.62/−0.62	0.72
5.5	34.9	LS-FM metal	inner	1.2/−1.2	0.75
			next-to-inner	0.30/−0.30	0.74
			outer	1.1/−1.1	0.71
			La7614		
1.5	12.9	LS-FM metal	inner	0.78/−0.78	0.81
			next-to-inner	0.62/−0.63	0.78
			outer	0.56/−0.57	0.74
2.7	89.82	LS-FM metal	inner	1.0/−1.0	0.81
			next-to-inner	0.56/−0.56	0.78
			outer	0.89/−0.89	0.74
4.0	81.9	LS-FM metal	inner	1.1/−1.1	0.79
			next-to-inner	0.44/−0.44	0.78
			outer	1.1/−1.1	0.73
5.5	27.4	LS-FM metal	inner	1.2/−1.2	0.77
			next-to-inner	0.33/−0.33	0.75
			outer	1.1/−1.1	0.71
			La112		
1.5	−122.4	LS-AFM metal		0.79/−0.79	0.85
2.7	−86.9	LS-AFM metal		0.83/−0.83	0.85
4.0	−63.0	LS-AFM metal		0.84/−0.84	0.84
5.5	−62.3	LS-AFM metal		0.70/−0.70	0.79

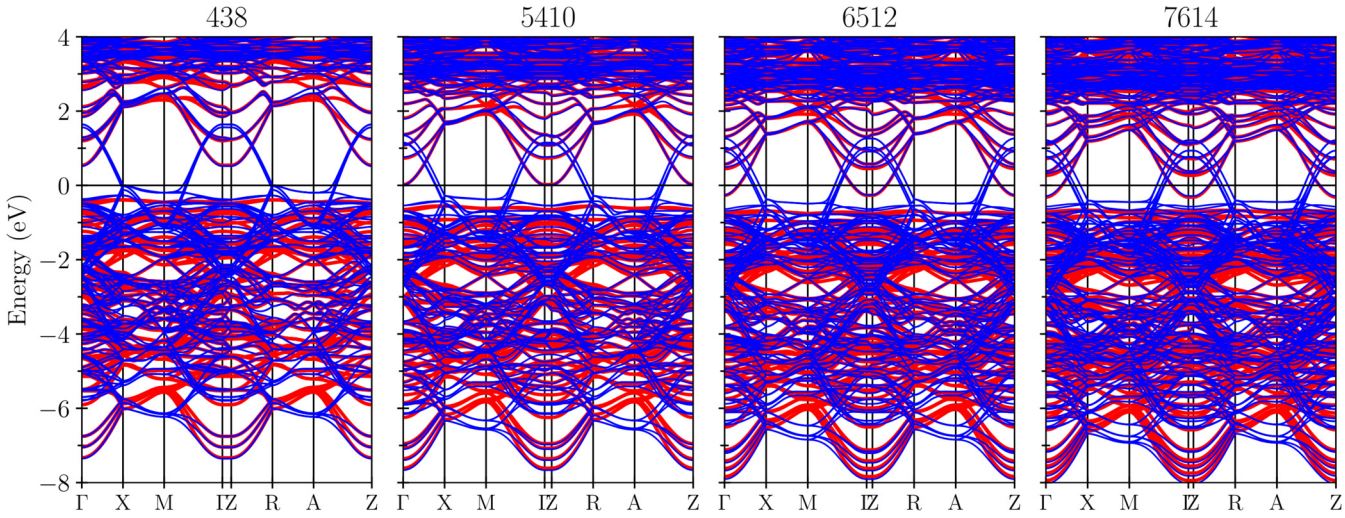

FIG. 6. Band structures of the $n = 3$–6 phases (left to right) from GGA + U (AMF) calculations within the LS-FM ground state at $U = 5.5$ eV. Blue (red) shows majority (minority) spin channels.

the ground state (GS) of each compound and the Ni magnetic moments for the AFM and FM configurations in all layers are also provided. The same information is provided in Table V for the AMF double counting scheme.

APPENDIX B: LS BAND STRUCTURES

The band structures from our GGA + U calculations for the LS-FM ground state of $n = 3$–6 layered nickelates within AMF for $U = 5.5$ eV are shown in Fig. 6. The majority (minority) spin channels are shown in blue (red). The evolution of the electronic structure as n increases repeats the same trends observed in the NM band structures shown in the main text. The La-5d bands begin playing a role in the La5410 ($n = 4$) compound and gradually increase their relevance in La6512 ($n = 5$) and La7614 ($n = 6$)—this effect is particularly noticeable at Γ.

[1] J. Bednorz and K. Müller, Z. Phys. B: Condens. Matter **64**, 189 (1986).
[2] V. I. Anisimov, D. Bukhvalov, and T. M. Rice, Phys. Rev. B **59**, 7901 (1999).
[3] K.-W. Lee and W. E. Pickett, Phys. Rev. B **70**, 165109 (2004).
[4] D. Li, K. Lee, B. Y. Wang, M. Osada, S. Crossley, H. R. Lee, Y. Cui, Y. Hikita, and H. Y. Hwang, Nature (London) **572**, 624 (2019).
[5] D. Li, B. Y. Wang, K. Lee, S. P. Harvey, M. Osada, B. H. Goodge, L. F. Kourkoutis, and H. Y. Hwang, Phys. Rev. Lett. **125**, 027001 (2020).
[6] V. V. Poltavets, K. A. Lokshin, S. Dikmen, M. Croft, T. Egami, and M. Greenblatt, J. Am. Chem. Soc. **128**, 9050 (2006).
[7] V. V. Poltavets, K. A. Lokshin, M. Croft, T. K. Mandal, T. Egami, and M. Greenblatt, Inorg. Chem. **46**, 10887 (2007).
[8] M. Greenblatt, Curr. Opin. Solid State Mater. Sci. **2**, 174 (1997).
[9] M. Crespin, P. Levitz, and L. Gatineau, J. Chem. Soc., Faraday Trans. 2 **79**, 1181 (1983).
[10] M. A. Hayward, M. A. Green, M. J. Rosseinsky, and J. Sloan, J. Am. Chem. Soc. **121**, 8843 (1999).
[11] A. Ikeda, T. Manabe, and M. Naito, Phys. C (Amsterdam) **495**, 134 (2013).
[12] A. Ikeda, Y. Krockenberger, H. Irie, M. Naito, and H. Yamamoto, Appl. Phys. Express **9**, 061101 (2016).
[13] M. Osada, B. Y. Wang, B. H. Goodge, K. Lee, H. Yoon, K. Sakuma, D. Li, M. Miura, L. F. Kourkoutis, and H. Y. Hwang, Nano Lett. **20**, 5735 (2020).
[14] K. Lee, B. H. Goodge, D. Li, M. Osada, B. Y. Wang, Y. Cui, L. F. Kourkoutis, and H. Y. Hwang, APL Mater. **8**, 041107 (2020).
[15] B. H. Goodge, D. Li, K. Lee, M. Osada, B. Y. Wang, G. A. Sawatzky, H. Y. Hwang, and L. F. Kourkoutis, Proc. Natl. Acad. Sci. USA **118**, e2007683118 (2021).
[16] M. Hepting, D. Li, C. J. Jia, H. Lu, E. Paris, Y. Tseng, X. Feng, M. Osada, E. Been, Y. Hikita, Y.-D. Chuang, Z. Hussain, K. J. Zhou, A. Nag, M. Garcia-Fernandez, M. Rossi, H. Y. Huang, D. J. Huang, Z. X. Shen, T. Schmitt *et al.*, Nat. Mater. **19**, 381 (2020).
[17] Y. Fu, L. Wang, H. Cheng, S. Pei, X. Zhou, J. Chen, S. Wang, R. Zhao, W. Jiang, C. Liu, M. Huang, X. Wang, Y. Zhao, D. Yu, F. Ye, S. Wang, and J.-W. Mei, arXiv:1911.03177.
[18] Q. Li, C. He, J. Si, X. Zhu, Y. Zhang, and H.-H. Wen, Commun. Mater. **1**, 16 (2020).
[19] B.-X. Wang, H. Zheng, E. Krivyakina, O. Chmaissem, P. P. Lopes, J. W. Lynn, L. C. Gallington, Y. Ren, S. Rosenkranz, J. F. Mitchell, and D. Phelan, Phys. Rev. Mater. **4**, 084409 (2020).
[20] Q. Gu, Y. Li, S. Wan, H. Li, W. Guo, H. Yang, Q. Li, X. Zhu, X. Pan, Y. Nie, and H.-H. Wen, Nat. Commun. **11**, 6027 (2020).
[21] P. Jiang, L. Si, Z. Liao, and Z. Zhong, Phys. Rev. B **100**, 201106(R) (2019).
[22] Y. Nomura, M. Hirayama, T. Tadano, Y. Yoshimoto, K. Nakamura, and R. Arita, Phys. Rev. B **100**, 205138 (2019).
[23] Z. Liu, Z. Ren, W. Zhu, Z. Wang, and J. Yang, npj Quantum Mater. **5**, 31 (2020).

[24] X. Wu, D. Di Sante, T. Schwemmer, W. Hanke, H. Y. Hwang, S. Raghu, and R. Thomale, Phys. Rev. B **101**, 060504(R) (2020).

[25] M.-Y. Choi, K.-W. Lee, and W. E. Pickett, Phys. Rev. B **101**, 020503(R) (2020).

[26] S. Ryee, H. Yoon, T. J. Kim, M. Y. Jeong, and M. J. Han, Phys. Rev. B **101**, 064513 (2020).

[27] Y. Gu, S. Zhu, X. Wang, J. Hu, and H. Chen, Commun. Phys. **3**, 84 (2020).

[28] I. Leonov, S. L. Skornyakov, and S. Y. Savrasov, Phys. Rev. B **101**, 241108(R) (2020).

[29] F. Lechermann, Phys. Rev. B **101**, 081110(R) (2020).

[30] F. Lechermann, Phys. Rev. X **10**, 041002 (2020).

[31] L.-H. Hu and C. Wu, Phys. Rev. Res. **1**, 032046(R) (2019).

[32] H. Sakakibara, H. Usui, K. Suzuki, T. Kotani, H. Aoki, and K. Kuroki, Phys. Rev. Lett. **125**, 077003 (2020).

[33] M. Jiang, M. Berciu, and G. A. Sawatzky, Phys. Rev. Lett. **124**, 207004 (2020).

[34] P. Werner and S. Hoshino, Phys. Rev. B **101**, 041104(R) (2020).

[35] H. Zhang, L. Jin, S. Wang, B. Xi, X. Shi, F. Ye, and J.-W. Mei, Phys. Rev. Res. **2**, 013214 (2020).

[36] Y.-H. Zhang and A. Vishwanath, Phys. Rev. Res. **2**, 023112 (2020).

[37] J. Karp, A. S. Botana, M. R. Norman, H. Park, M. Zingl, and A. Millis, Phys. Rev. X **10**, 021061 (2020).

[38] A. S. Botana and M. R. Norman, Phys. Rev. X **10**, 011024 (2020).

[39] Y. Wang, C.-J. Kang, H. Miao, and G. Kotliar, Phys. Rev. B **102**, 161118(R) (2020).

[40] V. V. Poltavets, M. Greenblatt, G. H. Fecher, and C. Felser, Phys. Rev. Lett. **102**, 046405 (2009).

[41] S. Sarkar, I. Dasgupta, M. Greenblatt, and T. Saha-Dasgupta, Phys. Rev. B **84**, 180411(R) (2011).

[42] J. Zhang, A. S. Botana, J. W. Freeland, D. Phelan, H. Zheng, V. Pardo, M. R. Norman, and J. F. Mitchell, Nat. Phys. **13**, 864 (2017).

[43] A. S. Botana, V. Pardo, and M. R. Norman, Phys. Rev. Mater. **1**, 021801(R) (2017).

[44] Q. Lei, M. Golalikhani, B. A. Davidson, G. Liu, D. G. Schlom, Q. Qiao, Y. Zhu, R. U. Chandrasena, W. Yang, A. X. Gray, E. Arenholz, A. K. Farrar, D. A. Tenne, M. Hu, J. Guo, R. K. Singh, and X. Xi, npj Quantum Mater. **2**, 10 (2017).

[45] Z. Li, W. Guo, T. T. Zhang, J. H. Song, T. Y. Gao, Z. B. Gu, and Y. F. Nie, APL Mater. **8**, 091112 (2020).

[46] P. Blaha, K. Schwarz, F. Tran, R. Laskowski, G. K. H. Madsen, and L. D. Marks, J. Chem. Phys. **152**, 074101 (2020).

[47] J. P. Perdew, K. Burke, and M. Ernzerhof, Phys. Rev. Lett. **77**, 3865 (1996).

[48] V. I. Anisimov, A. I. Poteryaev, M. A. Korotin, A. O. Anokhin, and G. Kotliar, J. Phys.: Condens. Matter **9**, 7359 (1997).

[49] E. R. Ylvisaker, W. E. Pickett, and K. Koepernik, Phys. Rev. B **79**, 035103 (2009).

[50] J. Zhang, Y.-S. Chen, D. Phelan, H. Zheng, M. R. Norman, and J. F. Mitchell, Proc. Natl. Acad. Sci. USA **113**, 8945 (2016).

[51] G.-M. Zhang, Y.-f. Yang, and F.-C. Zhang, Phys. Rev. B **101**, 020501(R) (2020).

[52] H. Sakakibara, K. Suzuki, H. Usui, S. Miyao, I. Maruyama, K. Kusakabe, R. Arita, H. Aoki, and K. Kuroki, Phys. Rev. B **89**, 224505 (2014).

[53] J. Q. Lin, P. Villar Arribi, G. Fabbris, A. S. Botana, D. Meyers, H. Miao, Y. Shen, D. G. Mazzone, J. Feng, S. G. Chiuzbăian, A. Nag, A. C. Walters, M. García-Fernández, K.-J. Zhou, J. Pelliciari, I. Jarrige, J. W. Freeland, J. Zhang, J. F. Mitchell, V. Bisogni *et al.*, Phys. Rev. Lett. **126**, 087001 (2021).

[54] C. Weber, C. Yee, K. Haule, and G. Kotliar, EPL **100**, 37001 (2012).

[55] F. C. Zhang and T. M. Rice, Phys. Rev. B **37**, 3759 (1988).

[56] S. W. Jang, T. Kotani, H. Kino, K. Kuroki, and M. J. Han, Sci. Rep. **5**, 12050 (2015).

[57] E. M. Nica, J. Krishna, R. Yu, Q. Si, A. S. Botana, and O. Erten, Phys. Rev. B **102**, 020504(R) (2020).

[58] We attempted to obtain estimates of the charge transfer energies for the $n = 3$–6 and ∞ compounds from the on-site energies of maximally localized Wannier functions (Ni $d_{x^2-y^2}$ and O $p\sigma$) derived using WANNIER90 [59,60]. We obtained well-localized Wannier functions (with spreads $\sim$1 Å^2) for the $n = 3$, 4, and ∞ materials using an energy window of -8 to 3 eV with the initial orbital projections being La-d_{xy}, La-d_{z^2}, all Ni-d, and O-p orbitals. For the $n = 5$ and 6 materials, we could not obtain well-localized Wannier functions. Therefore we present the charge transfer energies obtained from the density-of-states-derived centroids for all materials for consistency.

[59] A. A. Mostofi, J. R. Yates, G. Pizzi, Y.-S. Lee, I. Souza, D. Vanderbilt, and N. Marzari, Comput. Phys. Commun. **185**, 2309 (2014).

[60] J. Kunes, R. Arita, P. Wissgott, A. Toschi, H. Ikeda, and K. Held, Comput. Phys. Commun. **181**, 1888 (2010).

[61] J. Kapeghian and A. S. Botana, Phys. Rev. B **102**, 205130 (2020).

[62] M.-Y. Choi, W. E. Pickett, and K.-W. Lee, Phys. Rev. Res. **2**, 033445 (2020).

[63] A. S. Botana, V. Pardo, W. E. Pickett, and M. R. Norman, Phys. Rev. B **94**, 081105(R) (2016).

[64] V. Pardo and W. E. Pickett, Phys. Rev. Lett. **105**, 266402 (2010).

[65] J. M. Tranquada, Ferroelectrics **177**, 43 (1996).

[66] N. Poirot, R. A. Souza, and C. M. Smith, Solid State Sci. **13**, 1494 (2011).

[67] Y.-S. Yi, Z.-G. Yu, A. R. Bishop, and J. T. Gammel, Phys. Rev. B **58**, 503 (1998).

[68] P. Wochner, J. M. Tranquada, D. J. Buttrey, and V. Sachan, Phys. Rev. B **57**, 1066 (1998).

[69] J. Zhang, D. M. Pajerowski, A. S. Botana, H. Zheng, L. Harriger, J. Rodriguez-Rivera, J. P. C. Ruff, N. J. Schreiber, B. Wang, Y.-S. Chen, W. C. Chen, M. R. Norman, S. Rosenkranz, J. F. Mitchell, and D. Phelan, Phys. Rev. Lett. **122**, 247201 (2019).

[70] S. Huangfu, Z. Guguchia, D. Cheptiakov, X. Zhang, H. Luetkens, D. J. Gawryluk, T. Shang, F. O. von Rohr, and A. Schilling, Phys. Rev. B **102**, 054423 (2020).

[71] V. V. Poltavets, K. A. Lokshin, A. H. Nevidomskyy, M. Croft, T. A. Tyson, J. Hadermann, G. Van Tendeloo, T. Egami, G. Kotliar, N. ApRoberts-Warren, A. P. Dioguardi, N. J. Curro, and M. Greenblatt, Phys. Rev. Lett. **104**, 206403 (2010).

[72] B. W. Statt and L. M. Song, Phys. Rev. B **48**, 3536 (1993).

[73] M. Karppinen and H. Yamauchi, Philos. Mag. B **79**, 343 (1999).

[74] A. Trokiner, L. Le Noc, J. Schneck, A. M. Pougnet, R. Mellet, J. Primot, H. Savary, Y. M. Gao, and S. Aubry, Phys. Rev. B **44**, 2426 (1991).

[75] H. Kotegawa, Y. Tokunaga, K. Ishida, G.-q. Zheng, Y. Kitaoka, H. Kito, A. Iyo, K. Tokiwa, T. Watanabe, and H. Ihara, Phys. Rev. B **64**, 064515 (2001).

[76] Y. Tokunaga, K. Ishida, Y. Kitaoka, K. Asayama, K. Tokiwa, A. Iyo, and H. Ihara, Phys. Rev. B **61**, 9707 (2000).